BIOLOGICAL
CRYSTALLOGRAPHY

Volume 71 (2015)

Supporting information for article:

A high-transparency, micro-patternable chip for X-ray diffraction analysis of microcrystals under native growth conditions

Thomas D. Murray, Artem Y. Lyubimov, Craig M. Ogata, Huy Vo, Monarin Uervirojnangkoorn, Axel T. Brunger and James M. Berger

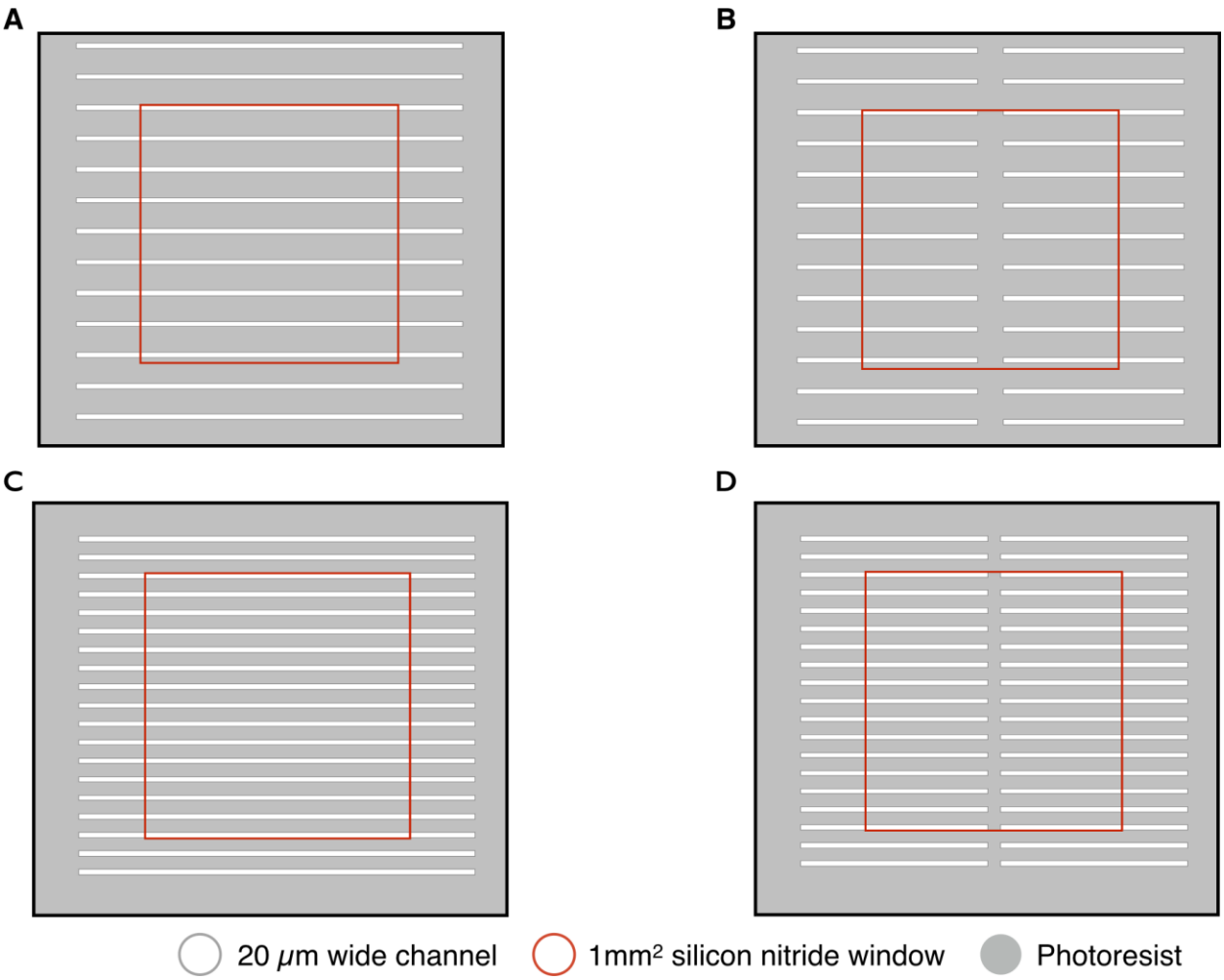

Figure S1 Channel chip designs. A-D) Schematic representations of 1 mm^2 silicon nitride window patterned with 20 μm wide photoresist channels.

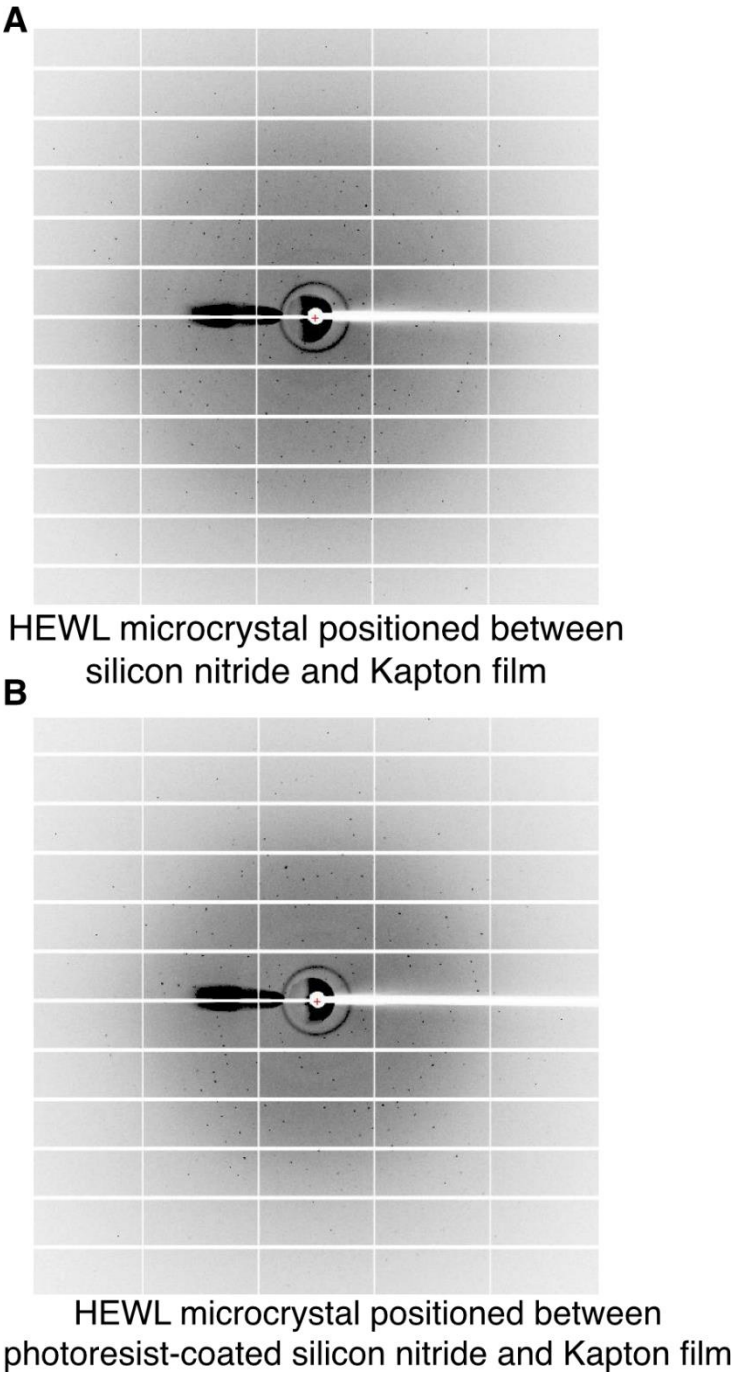

Figure S2 HEWL diffraction images from SSRL comparing the diffraction quality of two different microcrystals based on location. A) X-ray diffraction pattern of a HEWL microcrystal situated between silicon nitride and Kapton film. B) X-ray diffraction pattern of a different HEWL microcrystal located between a photoresist-coated portion of silicon nitride and Kapton film. The dark scattering ring at 16 Å in both A. and B. derives from the Kapton film.

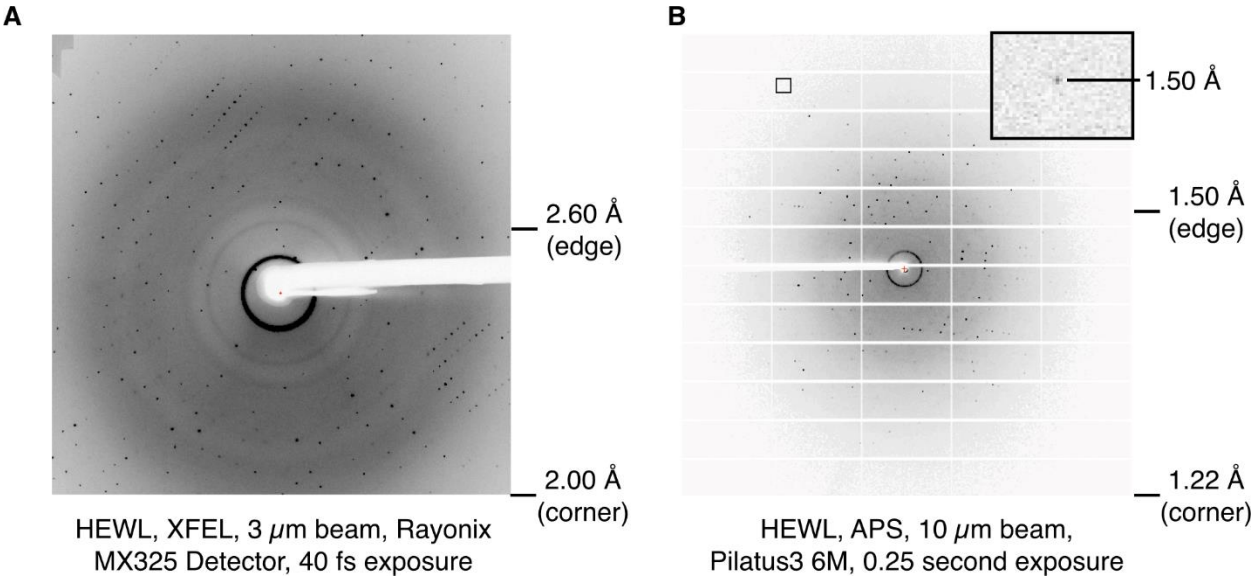

Figure S3 Diffraction from HEWL microcrystals within a three-layer device. A) Representative diffraction pattern from a 10-15 μm HEWL microcrystal collected at the XPP endstation of the LCLS using a 3 μm beam and a 40 fs beam pulse. B) Representative diffraction pattern from a 10-15 μm HEWL microcrystal collected at APS GMCA beamline 23 ID-D using a 10 μm beam and 0.25 s exposure. Inset: close-up of a diffraction peak measure at ~1.5 Å resolution. The dark scattering ring at 16 Å in both A. and B. derives from the Kapton film.

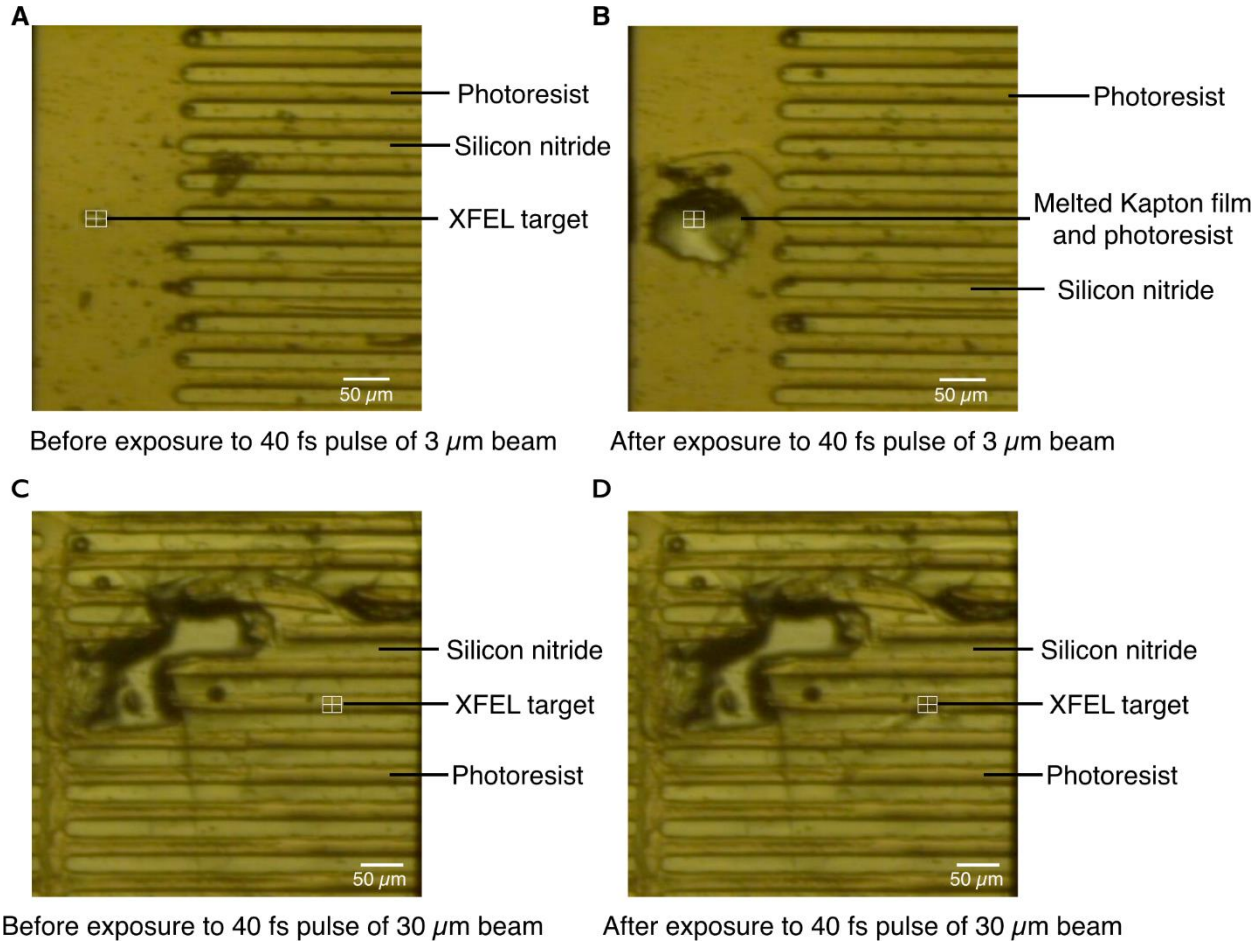

Figure S4 Performance of device materials with various XFEL beam sizes. Before and after pictures of channel-based chips used for XFEL data collection A) Picture of a chip prior to exposure with a 3 µm beam. B) Picture of a chip after exposure to a 40 fs pulse of a 3 µm, unattenuated beam. C) Picture of a chip prior to exposure using a 30 µm beam. D) Picture of a chip following exposure to a 40 fs pulse of a 30 µm beam.

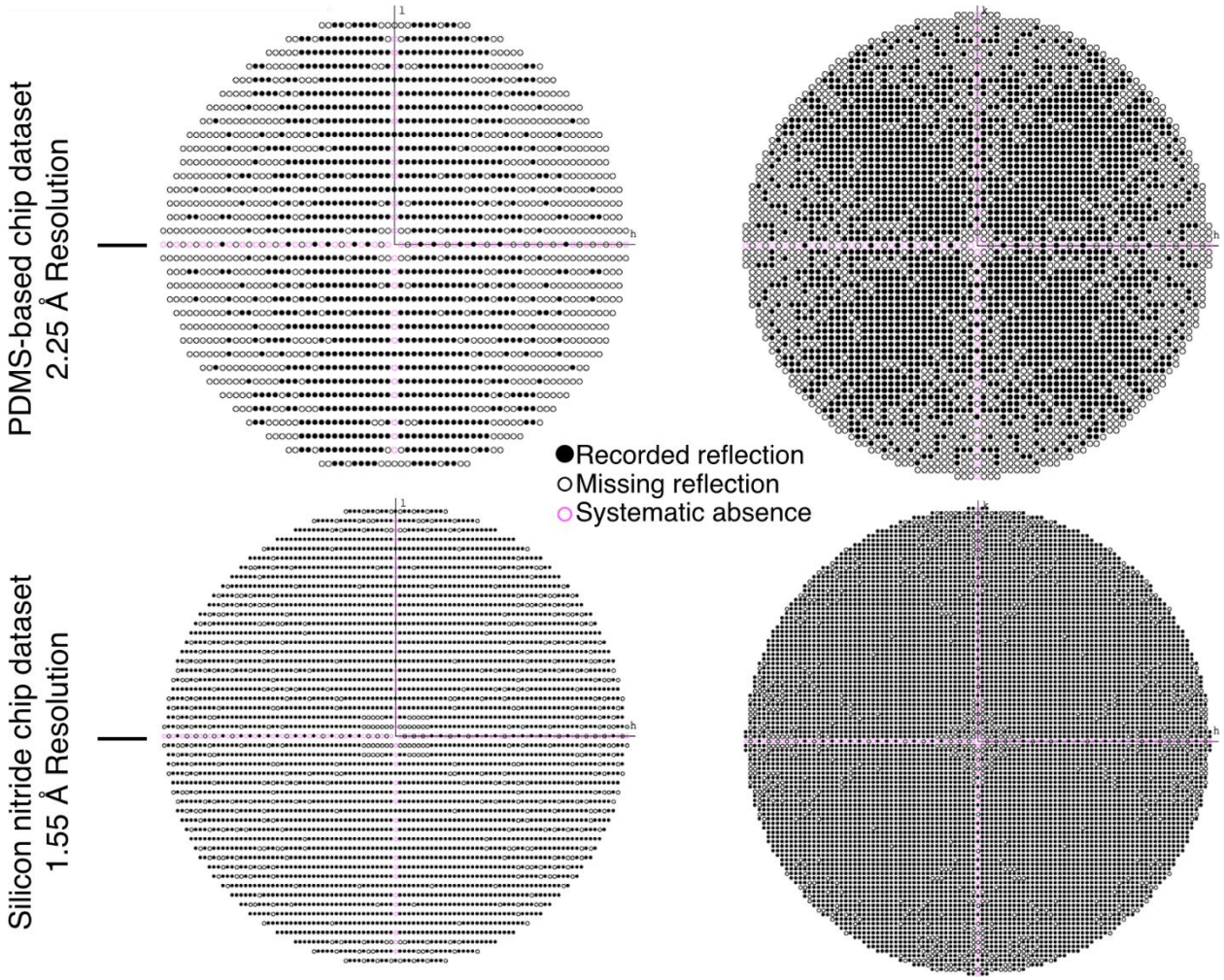

Figure S5 Comparison of completeness of silicon nitride device-derived and PDMS device-derived HEWL structures. 2D, reciprocal space plots (*h0l* layer) showing recorded and missing reflections are for HEWL datasets collected from either: A) a PDMS-based, microfluidic crystal capture device (Lyubimov *et al.*, 2015) or B) the three-layer silicon nitride-based device shown here.

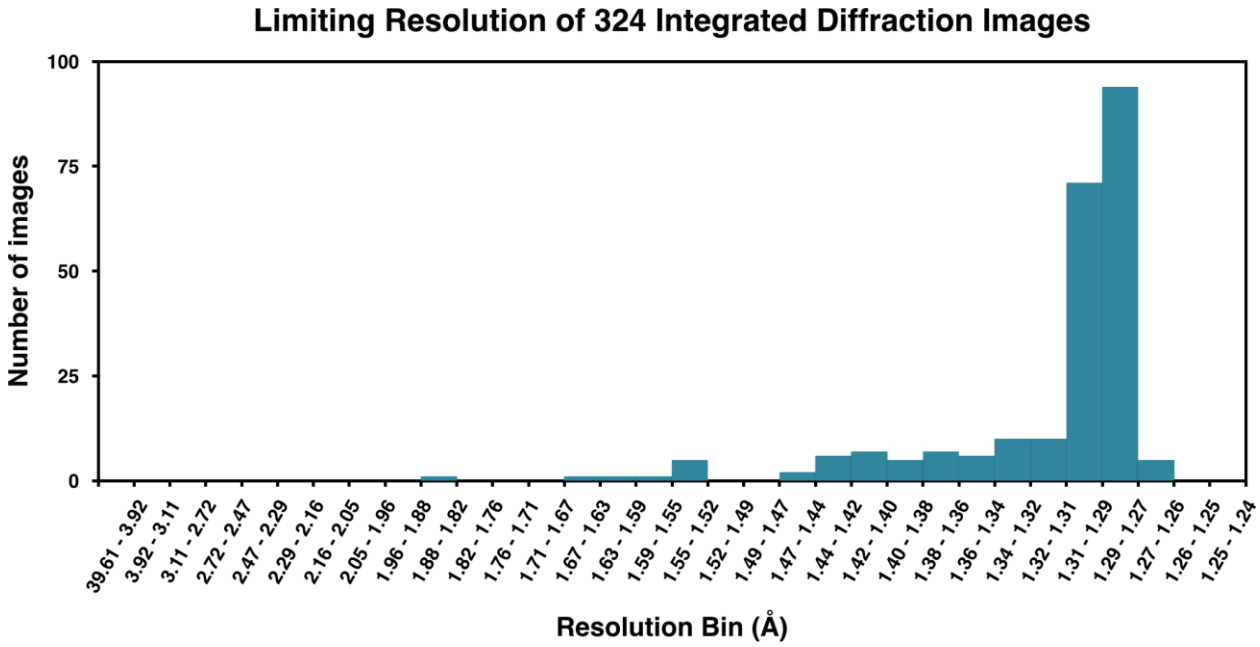

Figure S6 Single microcrystal diffraction limits. Histogram showing the limiting resolution of the 324 integrated images collected from three-layer chips and used for structure determination and refinement.

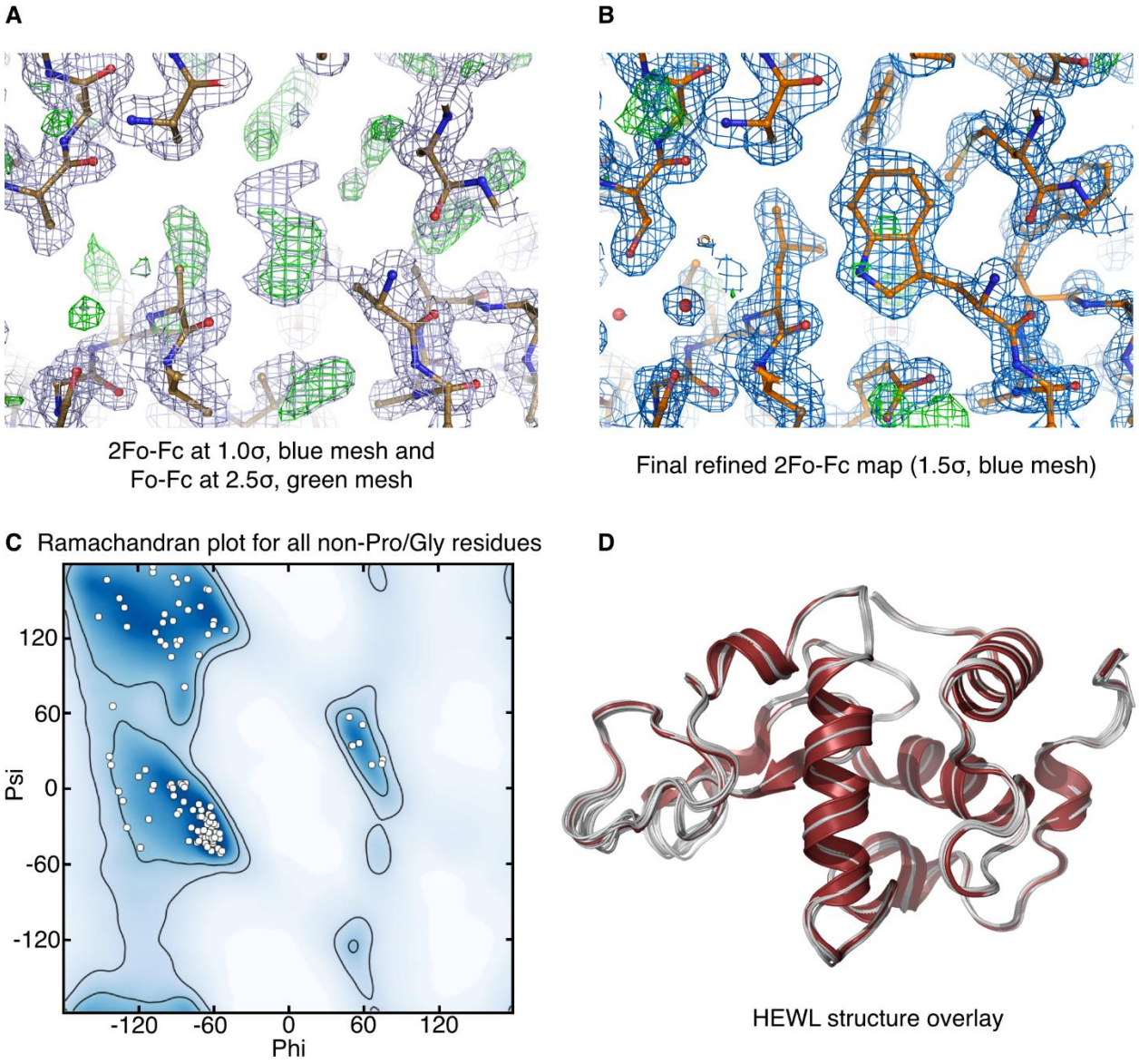

Figure S7 Determination and refinement of silicon nitride chip-derived HEWL structure. A) Electron density maps (2mFo-DFc at 1.0 σ, blue mesh and mFo-DFc at 2.5σ, green mesh) obtained from molecular replacement. B) Final refined 2mFo-DFc map (1.5σ, blue mesh) of tetragonal HEWL at 1.55 Å resolution. C) Ramachandran plot of all amino acid residues in the asymmetric unit. D) Superposition of tetragonal HEWL structure determined from in-chip diffraction data (red) vs. 15 tetragonal HEWL structures randomly drawn from the Protein Data Bank (grey).